

Evaluating adhesive bonding properties of T-joint between 3D printed stiffener and CFRP laminate manufactured by VARTM

By

Gauravkumar Raval

*Thesis
Submitted to Flinders University
for the degree of*

Master of Engineering (Mechanical)

Flinders University

13/06/2024

TABLE OF CONTENTS

TABLE OF CONTENTS	I
ABSTRACT	III
DECLARATION	IV
ACKNOWLEDGEMENTS	V
LIST OF FIGURES	VI
LIST OF TABLES	VI
1. INTRODUCTION	1
1.1 Aim and Objectives.....	2
2. LITERATURE REVIEW	3
2.1 Previous studies on composite T-joints and configurations.....	3
2.2 Selection of carbon fibre fabric and fabrication orientation of skin part.....	4
2.3 Selection of material for 3D printing, 3D printing technology and fabrication orientation of stiffener and flange part.....	4
2.4 T-joints manufacturing process (VARTM process).....	4
2.5 Testing methods.....	5
2.6 Research Gap	6
3. METHODOLOGY	6
3.1 Material details	6
3.2 3D printing.....	6
3.2.1 3D-printed stiffener and flange part.....	7
3.3 VARTM method.....	8
3.3.1 Manufacturing simple and modified adhesive-bonded T-joints	8
3.3.2 Manufacturing CFRP Skin part.....	9
3.4 Testing methods.....	10
3.4.1 Tensile Testing.....	10
3.4.2 Shear Testing.....	11
3.4.3 3-point Bending Testing	11
3.4.4 Electronic Microscopy Testing.....	11
3.5 Data Analysis (Evaluation).....	11
4. RESULTS	13
4.1 3D-printed flange part and CFRP skin part samples:	13
4.2 Simple and modified adhesive-bonded T-joints samples (PLA material):	15
4.3 Simple and modified adhesive-bonded T-joints samples (PA12-CF material):	16
4.4 Electronic Microscopy Images:	18
5. DISCUSSION	18
6. FUTURE TRENDS	22
7. CONCLUSION	22
REFERENCES	23

ABSTRACT

T-joints play a crucial role in various industries because of their outstanding mechanical properties and adaptability. This study focuses on the adhesive bonding properties of 3D-printed stiffener with CFRP (Carbon Fibre-reinforced Polymer) skin. Adhesive bonding between 3D-printed stiffener and CFRP laminates made with epoxy resin infusion occurs through the VARTM (Vacuum-assisted Resin Transfer Molding) process. 3D-printed parts were fabricated by Fused Deposition Modeling (FDM) printing technology. The study assessed the tensile strength and bending strength of PLA and PA12-CF materials, which are used for 3D printing the stiffeners. This study also evaluated the tensile strength and shear strength of simple adhesive-bonded T-joints and modified adhesive-bonded T-joints of 3D-printed stiffeners with CFRP laminates. Modified adhesive-bonded T-joints outperform simple adhesive-bonded T-joints due to the one carbon fibre fabric overlap on the flange part of the stiffener. PLA material provided excellent adhesion and made a better adhesive bond with carbon fibre fabric and epoxy resin. PA12-CF material has high tensile and shear strength, but it is weak when made to bond with CFRP skin with epoxy. The findings of this study provide information on the adhesive bonding characteristics of T-joints, which are made of CFRP laminate and 3D printing components. Overall, this research contributed to a better understanding of the performance and suitability of adhesive-bonded T-joints, particularly including 3D-printed components for engineering applications.

Keywords: T-joint, Plain weave carbon fibre fabric, Adhesive bond, VARTM, 3D printing, PLA, PA12-CF, FDM, CFRP laminate.

DECLARATION

I certify that this thesis:

1. does not incorporate without acknowledgment any material previously submitted for a degree or diploma in any university
2. and the research within will not be submitted for any other future degree or diploma without the permission of Flinders University; and
3. to the best of my knowledge and belief, does not contain any material previously published or written by another person except where due reference is made in the text.

Signature of student: *gauravkumar raval*

Print name of student: Gauravkumar Raval

Date: 13/06/2024

I certify that I have read this thesis. In my opinion it is fully adequate, in scope and in quality, as a thesis for the degree of Master of Engineering (Mechanical). Furthermore, I confirm that I have provided feedback on this thesis and the student has implemented it fully.

Signature of Principal Supervisor: *Youhong Tang*

Print name of Principal Supervisor: Prof. Youhong Tang

Date: 13/06/2024

ACKNOWLEDGEMENTS

First and foremost, I would like to express my deep appreciation to my supervisor, Prof. Youhong Tang, for his invaluable guidance and support throughout this project. His profound knowledge, insightful guidance, and constructive suggestions were instrumental in the successful completion of this research. Thank you again for your exceptional guidance and support.

I would like to express my appreciation to Flinders University's Tonsley campus for providing access to laboratory and testing facilities, which were key to obtaining the test results. I would also like to thank the Engineering services team of the Tonsley campus and Mr. Tim Hodge for their outstanding support and assistance during the fabrication and testing phase of this project.

Additionally, I want to express my gratitude to Rahul Prakash and Dineth Fernando for their support and assistance. Lastly, I would like to thank all those who have supported me directly or indirectly throughout this research.

LIST OF FIGURES

Figure 1: Composite stiffener-to-skin T-joint.....	1
Figure 2: Dimension of the 3D-printed Stiffener part	7
Figure 3: Dimension of the 3D-printed flange part.....	8
Figure 4: (A) Different layers inside the vacuum bag and (B) Experimental VARTM process	8
Figure 5: Dimension of simple adhesive-bonded T-joint.....	9
Figure 6: Dimension of modified adhesive-bonded T-joint.....	9
Figure 7: Dimension of CFRP skin part	10
Figure 8: (A) Tensile testing experimental setup (B) Shear testing experimental setup (C) 3-point bending testing experimental setup.....	10
Figure 9: Tensile testing of 3D-printed flange part and CFRP skin part.....	14
Figure 10: 3-point bending testing of 3D-printed flange part and CFRP skin part	14
Figure 11: Tensile testing of T-joint samples (PLA material)	15
Figure 12: Shear testing of T-joint samples (PLA material)	16
Figure 13: Tensile testing of T-joint samples (PA12-CF material).....	17
Figure 14: Shear testing of T-joint samples (PA12-CF material).....	17
Figure 15: Voids on the adhesive-bonded surface	18
Figure 16: Ultimate tensile strength of 3D-printed flange part and CFRP skin part.....	18
Figure 17: 3-point bending strength of 3D-printed flange part and CFRP skin part.....	19
Figure 18: Ultimate tensile strength of T-joint samples.....	19
Figure 19: Maximum shear strength of T-joint samples.....	20
Figure 20: (A) Tensile testing of modified adhesive-bonded T-joints (PLA material) (B) Shear testing of modified adhesive-bonded T-joints (PLA material) (C) Tensile testing of modified adhesive-bonded T-joints (PA12-CF material) (D) Shear testing of modified adhesive-bonded T-joints (PA12-CF material).....	21

LIST OF TABLES

Table 1: 3D printing process parameters	7
Table 2: Tensile testing and shear testing of 3D-printed flange part of PLA and PA12-CF material and CFRP skin part.....	13
Table 3: Tensile testing and shear testing of T-joint samples of PLA material	15
Table 4: Tensile testing and shear testing T-joint samples of PA12-CF material	17

1. INTRODUCTION

Composite materials are becoming a popular choice in many industries due to their excellent mechanical properties and diversity of characteristics [1]. T-joints can be found at the interfaces between composite spars, ribs, bulkheads, and skin. Figure 1 indicates the web is connected to the substructure, the flange interacts with the skin, and the filler radius supports the transfer of load between the web and flange. The main goal of the T-joints is to transfer different stresses to the skin part. The skin part of the T-joint is made using plain weave carbon fibre infused with epoxy. This skin part acts as the horizontal component of the T-joint structure. When carbon fibre fabric is combined with epoxy, it forms a strong composite material with enhanced strength, durability, and resistance to environmental factors. This horizontal skin part is necessary for providing the structural support needed to evaluate the adhesive bond strength of the T-joint [2].

Figure removed due to copyright restriction.

Figure 1: Composite stiffener-to-skin T-joint

Source: (Sapi,2019)

In recent years, the integration of additive manufacturing technologies with traditional composite materials has led to significant advancements in the field of advanced manufacturing. Composite T-joint structures have found various applications in the fields of automobiles, aerospace, and marine industries over an extended period. Traditionally, both the stiffener and skin part of T-joints are made from carbon fibre composites. This thesis explores the inclusion of FDM 3D printing and VARTM process for the production and assessment of composite T-joints. FDM, a 3D printing technique, utilises thermoplastic filaments such as Polylactic Acid (PLA) and Polyamide 12 Carbon Fibre (PA12-CF) to produce stiffener and flange components. PLA is very much suitable for 3D printing because of its good printing dimensional stability and ease of printing, whereas PA12-CF has exceptional strength because of carbon fibre reinforcement [3] [4]. Plain weave carbon fibre

fabrics are used in the skin part due to their high mechanical properties [5]. VARTM is a composite manufacturing process used to fabricate very high-quality and lightweight composites with complex geometries [6]. A thorough testing procedure is set up to assess the mechanical properties of the T-joints. The Instron 5969 Universal Testing Machine (UTM) is used to conduct tensile and shear strength tests to quantify the adhesive bonding strength of the T-joints [7] [8]. The study seeks to assess the bonding strength of simple adhesive bonds in comparison to modified adhesive bonds that include an extra layer of carbon fibre reinforcement on the flanges part. By focusing on results obtained from mechanical testing, this research aims to provide insights into the effectiveness of integrating 3D-printed components with CFRP manufactured using VARTM. The results of this research will be beneficial in the enhancement of manufacturing processes and the creation of tougher and lighter composites that can be used in various fields.

1.1 Aim and Objectives

Aim: This project focuses on evaluating the adhesive bonding properties of the T-joints between 3D printed part and CFRP laminates manufactured by using VARTM process.

Objectives:

- Understand the structural challenges of T-joints in composite materials and analyse the different T-joint configurations employed in fabricating composite materials.
- Using PLA and PA12-CF for the manufacture of the stiffener parts and flange parts using 3D printing.
- Manufacturing simple adhesive-bonded T-joints and modified adhesive-bonded T-joints between 3D-printed part and CFRP sheets with epoxy, and CFRP skin part using VARTM process.
- To conduct tensile and 3-point bending testing of 3D-printed flange parts and CFRP skin parts separately.
- To conduct tensile and shear strength tests on T-joints using the Instron Universal Testing Machine to check the adhesive bonding strength of the T-joints.
- Compare the strengths of simple and modified adhesive-bonded T-joints to determine which type provides better bonding strength.
- Compare the adhesive bonding strengths of T-joint samples of both PLA and PA12-CF materials to assess which material provides good bonding strength with CFRP skin.

2. LITERATURE REVIEW

2.1 Previous studies on composite T-joints and configurations

Cardoso et al. (2018) conducted pull-off tests on a T-shaped joint made from CFRP, which was bonded using adhesive to attach a stiffener to a flat piece of CFRP. The study's findings, which are relevant to the current research, include a better understanding of the failure of the T-joint, aiding in the selection of an appropriate T-joint design [9].

Sapi et al. (2019) found that the analysis and fabrication of composite T-joints depend on factors such as filler radius, web dimensions, and flange thickness to achieve the desired design and testing outcomes. T-joint specimens typically have a standard width of 20 mm, this dimension effectively reduces stress concentrations near the edges and maintains a more uniform stress distribution in the middle section of the specimen. The flange and the web of the T-joint are designed to have a constant thickness and width to ensure that the stress is distributed evenly under tensile load. In the case of tensile testing, the height of the specimen does not affect the strength of the joint. The research revealed that filler radius strongly impacts the load-bearing capability and stress distribution in the T-joint. Further, if the value of the filler radius is larger, the load is distributed effectively so that the joint strength is also high. This general understanding of the dimensions of the stiffener section and filler geometry from this research is valuable for designing composite T-joints, which aligns with the current study [10].

Cope et al. (1982) studied the design of different T joints and identified the T joint with high tensile strength. The design involves a thin spar co-cured with a thick wing skin placed perpendicularly. This study achieved significant improvement in out-of-plane strength by adjusting the overlap geometry. By comparing T-joints with different filler radius, the study found that the T-joint with a filler radius of 12.5 mm offered the highest tensile strength. This study also proved that, as the base of the spar and filler radius of the joint increases, the bonding strength of the T-joint also increases. These findings support the current research by providing the T-joint configuration base part and the appropriate filler radius value [11].

Zhang et al. (2014) studied the interaction of overlaminates on the mechanical response of all-composite μ -joints. Researchers found that incorporating the carbon fibre overlaminates increases the joint strength. In the current research, modified adhesive-bonded T-joints were fabricated based on these findings with one layer of carbon fibre fabric overlapping the

stiffener flange. This method increases the joint strength of the T-joint to withstand varying mechanical loads [12].

2.2 Selection of carbon fibre fabric and fabrication orientation of skin part

The study by Patel et al. (2023) highlights several important aspects of the selection and orientation of carbon fibre fabrics for skin part, aligning with current research. This study examined the influence of stacking sequence and fibre orientation on the mechanical behaviour of the composites made from plain weave fibre fabrics through the VARTM process. In this study, researchers investigated an array of fibre orientations such as $0^{\circ}/90^{\circ}$, $15^{\circ}/75^{\circ}$, $30^{\circ}/60^{\circ}$, and $45^{\circ}/-45^{\circ}$. The study determined that $0^{\circ}/90^{\circ}$ fibre orientation provided the highest tensile and flexural strength among all fabric orientations. Of all the orientations, the $45^{\circ}/-45^{\circ}$ had the least tensile and flexural strength. This study proved that the carbon fibre orientation plays a major role in determining the mechanical properties of the composites [5].

2.3 Selection of material for 3D printing, 3D printing technology and fabrication orientation of stiffener and flange part

Hiremath et al. (2023) investigated that the fabrication orientation affected the tensile and shear properties of PLA samples printed through the FDM printing process. FDM is a 3D printing process that fabricates the 3D-printed parts by adding material layer by layer. Researchers revealed that by combining a 100% infill density with a 0° print orientation, PLA lap joints have higher tensile strength to a 90° or 45° orientation. Findings from this research study help the current study by aiding in the selection of an appropriate 3D printing material, fabrication orientation, 3D printing technology and, infill density, for achieving the best mechanical properties of 3D-printed parts [13].

Pejkowski et al. (2023) determined the mechanical properties of reinforcing PA12 with carbon fibres and glass bubbles. PA12-CF is a nylon/carbon fibre composite filament that provides a practically superior material compared to standard PA12 because carbon fibre enhances the mechanical properties. In this study, the PA12-CF specimen has a higher tensile strength and creep resistance than PA12CF-AM and PA12 polyamide. This research offers insights into the selection of materials for 3D-printed parts in the current study [4].

2.4 T-joints manufacturing process (VARTM process)

Tamakuwala et al. (2021) introduced VARTM, a technical method of manufacturing composite materials with high productivity, a low void ratio, and accuracy to produce a fibre-reinforced polymer component. Several Liquid Composite Moulding techniques, such as hand lay-up, spray-up, filament winding, pultrusion, RTM, VARTM, S-CRIMP, and ICM, are used for manufacturing polymer composites. In the VARTM method, dry fibre reinforcement materials, including carbon fibre or glass fibre, are stacked into the mould and covered by a vacuum bag. A vacuum is then applied to the mould which in turn has a certain pressure difference acting on the fibre preform, which forces the liquid resin to flow through the fibre preform and wet the fibres accordingly. These fibre-reinforced resins are then taken through the process of curing to produce a rigid composite piece. The findings help current research enhance the knowledge of the manufacturing processes for creating T-joint samples that are durable and lightweight for various uses [6].

Kumar et al. (2022) discovered that resin flow significantly affects composite part quality and properties. The recommended VARTM pressure range is 60-70 kPa. Excessive pressure can cause voids and defects due to increased resin flow, while low pressures may limit fibre saturation. These findings were useful in maintaining the resin flow and vacuum pressure during VARTM in the current research.[14].

2.5 Testing methods

Dahmen et al. (2019) studied the fabrication of hybrid composites T-joints by co-curing with 3D-printed dual-cure epoxy. In this study, tensile tests were conducted with a controlled loading rate of 2 mm/min to evaluate the mechanical properties of the composite T-joint [7]. Liu et al. (2021) examined the T-joints in composite sandwich structures under shearing and bending testing. The shear testing procedure involves subjecting the samples to a shear loading rate of 2 mm/min. This controlled loading rate helps to accurately capture the mechanical behaviour of the T-joints under shear load [8]. Sun et al. (2021) examined the mechanical behaviour of carbon fibre/honeycomb sandwich panels at different loading rates. This study provides information about the experimental setup method for three-point bending testing at a loading rate of 2 mm/min [15]. These studies provide insights into the experimental setups and methodologies for tensile, shear, and bending tests, all using the same loading rate of 2 mm/min, which is relevant to the current study. The study conducted by Zhao et al. (2011) highlights electronic microscopy approach enables the determination of atomic structure of carbon nanotubes. This study helps the current research to select an

appropriate technique for checking the quality of adhesive-bonded T-joint surfaces after tensile and shear testing [16].

2.6 Research Gap

There is limited research on the adhesive bond strength of T-joints formed between 3D-printed stiffener and CFRP-based skin sections manufactured using the VARTM process. This study aims to research different designs and configurations of composite T-joints and to assess their adhesive bonding strength through mechanical testing. Two different materials for 3D printing the stiffener sections, namely PLA and PA12-CF, are assessed through mechanical testing to identify the material's tensile strength and the adhesion bonding characteristics of both materials. The study also examines the bond surface between the 3D-printed stiffener and skin sections to analyse the contact surface and the presence of voids. The impact voids have on the adhesive bonding strength between the composite and 3D printed parts is assessed. A comparison study on the impact of adding a carbon fibre sheet overlap to the flange section versus simple adhesion bonding methods to evaluate the change in strength for both.

3. METHODOLOGY

3.1 Material details

This study uses the ATL Composites ZP200, a plain weave carbon fabric with a weight of 200 gsm, a thickness of 0.5 mm, and a weave pattern of 3k [17]. This study uses two parts of the epoxy material: part A is resin (KINETIX RD246), and part B is hardener (KINETIX HD160). For weight purposes, the epoxy resin system has a ratio of 80:20 per 100 ml of resin mixture to the hardener [18]. Two types of 3D printed materials are used to fabricate the stiffener parts of the T-joints, PolyLite™ PLA and PolyMide™ PA12-CF Materials. PolyLite™ PLA material with a 1.75 mm diameter filament was regular and white, and 1 kg per spool [19]. PolyMide™ PA12-CF Materials filament with a 2.85 mm diameter of black colour and 500 grams per spool [20].

3.2 3D printing

AUTODESK Inventor Professional 2024 was utilized for drawing the 3D parts. The printing process involves preparing the 3D printer with the right settings such as temperature control settings, fabrication orientation, and speed that enables high quality and dimensional accuracy of the stiffener parts. 3D printing process parameters for the stiffener part of both

materials PLA and PA12-CF are shown in Table 1. FDM 3D printing technology is used to fabricate the stiffener part of both materials. After fabricating the stiffener parts using the 3D printing, the parts are checked for defects, including any form of imperfection that may affect the bonding process later [3].

3.2.1 3D-printed stiffener and flange part

Figure removed due to copyright restriction.

Table 1: 3D printing process parameters

Source: www.3dprintingsolutions.com

The parameters, such as the thickness and length of the 3D-printed stiffener part, are important to ensure the structural stability of the part. The stiffener part is designed with a specific length of 150 mm, width of 20 mm and height of 100 mm, as indicated in Figure 2. These dimensions are chosen to provide enough bonding area with the CFRP skin part and enough structural support within the T-joint assembly [10] [11] [21]. The 3D-printed parts are taken out directly from the 3D printing machine and used in the further VARTM process to create T-joints without any surface finish treatments on the base section.

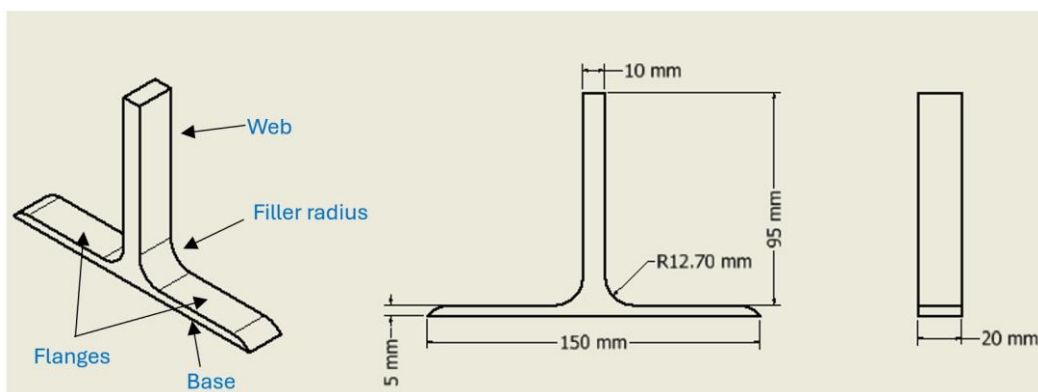


Figure 2: Dimension of the 3D-printed Stiffener part

During tensile and shear testing, the maximum force is applied to the stiffener flanges and base to assess T-joint tensile and shear strength. For consistency, the stiffener flange part is printed using the same process parameters for both PLA and PA12-CF materials. The

stiffener flange is of uniform cross-section, and its dimensions are 150 mm in length, 20 mm in width, and 5 mm in thickness, as shown in Figure 3. [10] [11] [21].

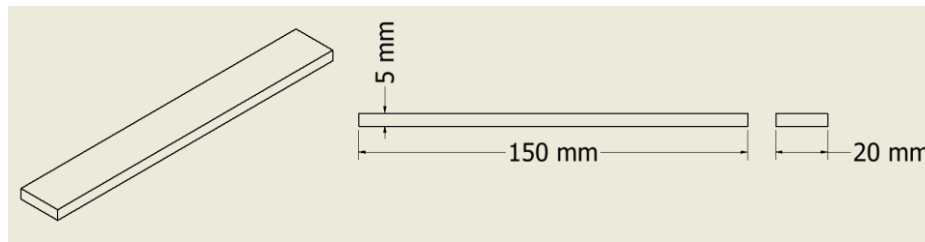


Figure 3: Dimension of the 3D-printed flange part

3.3 VARTM method

3.3.1 Manufacturing simple and modified adhesive-bonded T-joints

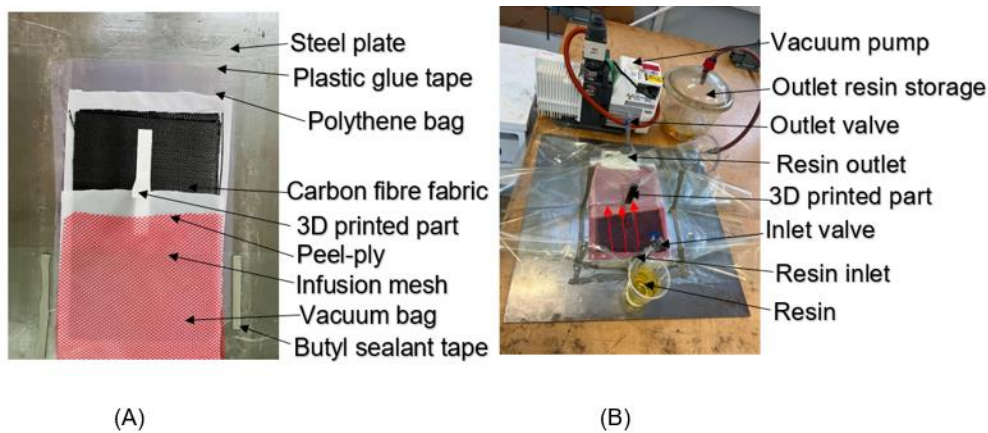


Figure 4: (A) Different layers inside the vacuum bag and (B) Experimental VARTM process
Source: Flinders University

The different layers inside the vacuum bag and the experimental VARTM process are shown in Figure 4. Firstly, the flat steel plate is used as the bottom surface, and the polythene bag is placed on it and sealed tightly with the help of plastic glue tape. The first layer is peel-ply placed on the polythene bag. Then, for the manufacturing of simple adhesive-bonded T-joints, five plain weave carbon fibre fabrics are stacked on peel-ply in sequence of 0°/90° [5]. The 3D-printed part was placed on the carbon fibre fabrics. On the other hand, for the manufacturing modified adhesive-bonded T-joints, four plain weave carbon fibre fabrics are stacked on peel-ply in the sequence of 0°/90°. Then, one carbon fibre fabric is accurately cut to have a width of 10 mm and a length of 20 mm to replicate the dimensions and shape of the top of the stiffener part. This fabric is placed on the setup, ensuring that it overlaps the stiffener flanges and its ends on the base layer [12].

Peel ply and infusion mesh are cut to the same dimensions as carbon fibre fabric and laid on the stiffener part. Infusion mesh is used to distribute the resin evenly on the fibre reinforcements. The vacuum bag is tightly sealed by using butyl sealant tape. Sealant tape

seals around all layers to eliminate any air leaks and retain the vacuum during resin infusion. The vacuum pump was started and the normal pressure of 60–70 kPa was provided by the vacuum pump. To begin with resin flow inside the vacuum bag, the setup process is put on hold for five minutes to examine the presence of any leaks that may result in the free flow of air during the process. Figure 4 illustrates the flow of resin inside the vacuum bag with the inlet valve open. The vacuum pump is then stopped and closed the inlet valve and outlet valve. The epoxy resin requires 28 hours of curing time at room temperature, which is sufficient to ensure that the resin is fully cured to offer good bonding strength with the carbon fibre reinforcement and the 3D-printed part [6].

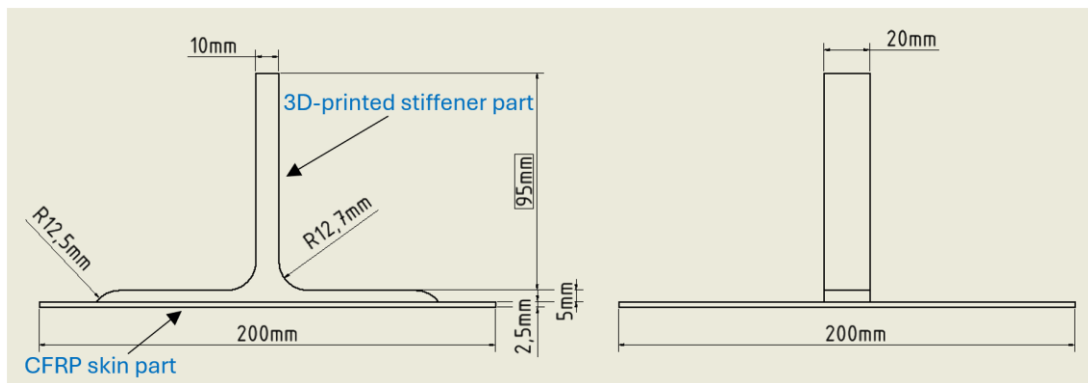


Figure 5: Dimension of simple adhesive-bonded T-joint

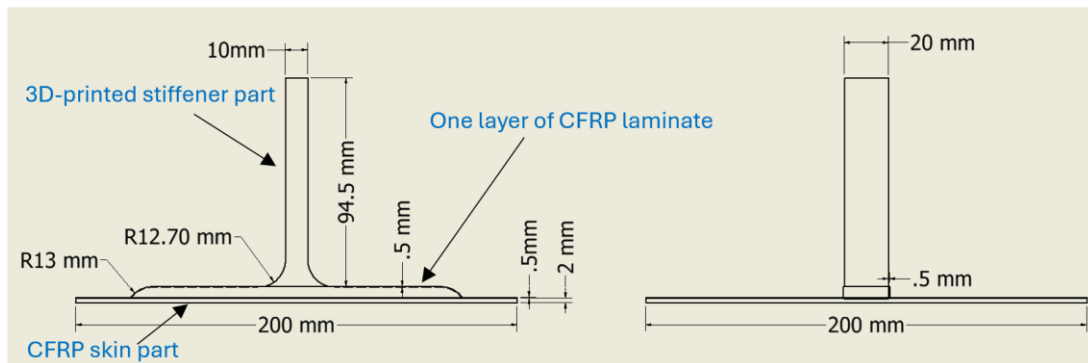


Figure 6: Dimension of modified adhesive-bonded T-joint

The structure and design of the simple adhesive-bonded T-joint and the modified adhesive-bonded T-joint are shown in Figure 5 and Figure 6, respectively. The simple adhesive-bonded T-joint has facilitated the continuation of the standard dimensions for stiffener and skin parts. The modified adhesive-bonded T-joint is incorporated with a 0.5 mm layer on the stiffener flanges. This may increase the joint's general solidity and stability [12]. This difference in the joint's construction allows the comparison of the mechanical characteristics and degree of bond formation.

3.3.2 Manufacturing CFRP Skin part

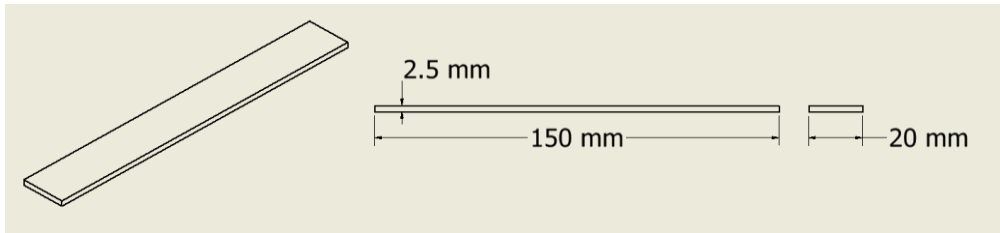


Figure 7: Dimension of CFRP skin part

In the VARTM process, the skin part is prepared by five plain weave carbon fiber fabrics bonded together with epoxy maintained to achieve the correct sizes and mechanical characteristics. Skin part dimensions are fixed at 300mm in length, 200mm in width, and 2.5mm in thickness. To get to the required sizes, the CFRP skin part is first cut into six pieces using AJAX Vertical Bandsaws, each with dimensions of 150mm in length, 20mm in width, and a thickness of 2.5mm, as shown in Figure 7. These cut pieces are perfectly oriented and piled, following the base of the 3-printed stiffener part.

3.4 Testing methods

3.4.1 Tensile Testing

The universal tensile testing machine (Instron 5969) conducts tensile tests of the T-joint to measure its tensile properties. Figure 8 (A) shows the experimental setup method for the tensile test. The 3D-printed stiffener part is fixed tightly to the upper fixture of the Instron machine. Steel plates and bolts firmly secured the skin to the platform of the testing machine, preventing any deformation or slippage during testing. The tensile test is conducted at a controlled loading rate of 2 mm/min, set in the testing machine until the T-joint fails. The maximum tensile load value and displacement value are measured from the load-displacement curve at the time of the occurrence of the T-joint failure [7]. In this study, a total of 21 samples tested using the UTM.

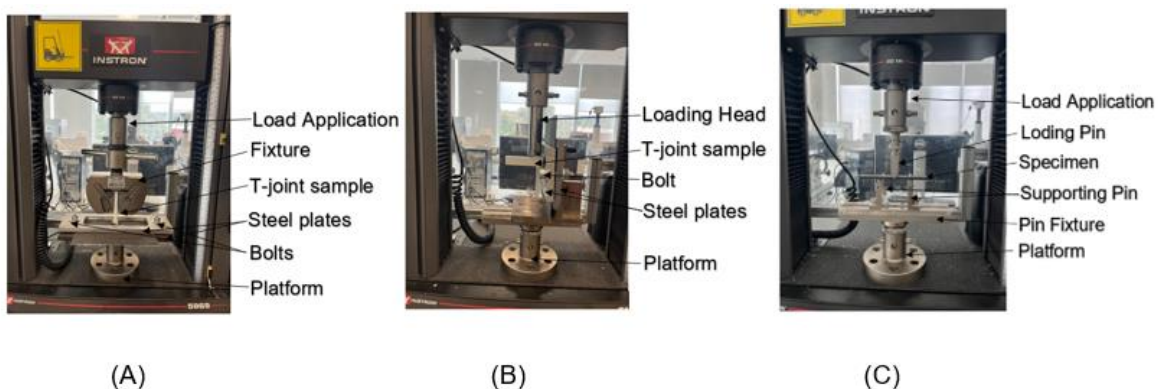


Figure 8: (A) Tensile testing experimental setup (B) Shear testing experimental setup (C) 3-point bending testing experimental setup

3.4.2 Shear Testing

The shear test T-joints are carried out on the UTM. The shear test experimental setup method is shown in Figure 8 (B). The CFRP skin portion is fastened between the steel plate holders of the test machine in this test. The Instron machine's loading head has a 20 mm diameter cylindrical end that aids in imparting a steady shear force to the T-joint. The shear test is run at a regulated loading rate of 2 mm/min until the T-joint breaks. The maximum shear load value and displacement value were measured from T-joint's load-displacement response [8]. In this study, the Instron machine is used to measure the shear strength of 12 T-joint samples.

3.4.3 3-point Bending Testing

The 3-point bending test of flange part and CFRP skin part were carried out using the Instron 5969 machine. The 3-point bending test experimental setup method shown in Figure 8 (C). The setup method for the 3-point bending test involves positioning the sample between two supporting pins spaced 50 mm apart. The supporting pins are connected to the platform through a pin fixture. The test is conducted at a controlled loading rate of 2 mm/min until the sample beaks. The maximum bending load value and displacement value were measured from sample's load-displacement response [15]. 3-point bending strength tests were conducted on a total of 9 samples.

3.4.4 Electronic Microscopy Testing

Zeiss Axiocam 305 colour electron microscope was used to take images of the adhesive bonding surface after tensile and shear testing of simple and modified adhesive-bonded T-joints. These images allow the examination of voids in the adhesive bond surface post-testing. The electron microscopy testing provides detailed visual insights into the microstructural integrity of the adhesive bond, highlighting any voids or defects that may arise due to improper resin flow or trapped air inside the vacuum bag [16]. This analysis helps understand the failure mechanisms and the quality of the adhesive bonding in the T-joint samples.

3.5 Data Analysis (Evaluation)

The load vs. displacement responses obtained from tensile, shear and 3-point bending tests provided insights into the mechanical behavior of the samples. The ultimate tensile strength and maximum bending strength of 3D-printed flange part and CFRP skin, and the ultimate tensile strength and maximum shear strength of adhesive-bonded T-joints are defined by

using load vs. displacement responses. This analysis process provided valuable information regarding the strength and failure mechanisms of the T-joint assemblies, aiding in the comprehensive evaluation of their mechanical properties.

For Stiffener Flanges and CFRP skin part:

$$\text{Ultimate tensile Stress } (\sigma_t) : \frac{P}{A} = \frac{P}{b \cdot d}$$

Here, P is the ultimate load at the sample failure in N, A is the cross-section area of sample in mm², b is the width of the sample in mm, d is the thickness of the sample in mm [22].

$$\text{Maximum bending stress } (\sigma_b) : \frac{Mc}{I}$$

$$M = \frac{PL}{4}, \text{ the moment in the sample.}$$

$$C = \frac{d}{2}, \text{ here d is the thickness of the sample in mm.}$$

$$I = \frac{bd^3}{12}, \text{ the second moment of inertia of the sample.}$$

$$\text{Maximum bending stress } (\sigma_b) : \frac{3PL}{2bd^2}$$

Here, P is the load at the sample failure in N, L is the span length in mm, b is the width of the sample in mm, d is the thickness of the sample in mm [23].

For simple and modified adhesive-bonded T-joint samples:

$$\text{Ultimate tensile stress } (\sigma_t) : \frac{Mc}{I}$$

$$M = \frac{PL}{4}, \text{ the moment in the T-joint sample.}$$

$$C = \frac{d}{2}, \text{ d is the thickness of the flange part in mm.}$$

$$I = \frac{db^3}{12}, \text{ the second moment of inertia of the flange part in the z axis.}$$

$$\text{Ultimate tensile stress } (\sigma_t) : \frac{3PL}{2b^3}$$

Here, P is the ultimate load at the sample failure in N, L is the span length in mm, b is the width of the sample [24]

$$\text{Maximum shear stress } (\sigma_b) : \frac{4.24 P A}{db^2}$$

Here, P is the load at the T-joint sample failure in N, A is the distance between the base to the point where the load is applied on the T-joint sample in mm, d is the thickness of the flange part in mm, b is the width of the T-joint in mm [25].

4. RESULTS

4.1 3D-printed flange part and CFRP skin part samples:

Tensile Testing				3-Point Bending Testing			
Samples	Maximum Tensile Load (N)	Displacement (mm)	Ultimate Tensile Strength (MPa)	Samples	Maximum Bending Load (N)	Displacement (mm)	Maximum Bending Strength (MPa)
3D-printed flange part (PLA Material):							
PLAT1	4348.93	2.31	43.48	PLAS1	441.63	4.65	66.24
PLAT2	4613.65	2.39	46.13	PLAS2	383.67	4.23	57.55
PLAT3	4355.52	2.43	43.55	PLAS3	438.72	4.59	65.80
Average	4439.36	2.37	44.38	Average	421.34	4.49	63.19
3D-printed flange part (PA12-CF Material):							
PAT1	6675.61	4.98	66.75	PAS1	548.29	8.23	82.24
PAT2	6753.18	5.21	67.53	PAS2	553.54	8.39	83.03
PAT3	6579.14	4.93	65.79	PAS3	557.78	7.79	83.66
Average	6669.3	5.04	66.69	Average	553.20	8.13	82.94
CFRP skin part:							
CFT1	15670.63	3.41	313.41	CFS1	281.82	8.72	169.09
CFT2	15574.97	3.32	311.49	CFS2	254.75	8.54	152.85
CFT3	16205.82	3.47	324.11	CFS3	251.64	8.12	150.98
Average	15817.13	3.40	316.33	Average	262.73	8.46	157.64

Table 2: Tensile testing and shear testing of 3D-printed flange part of PLA and PA12-CF material and CFRP skin part

Tensile testing and 3-point bending testing have been performed on various materials, and their results values are presented in Table 2. Figure 9 and Figure 10 show graphs of the testing results of various materials for tensile testing and 3-point bending testing, respectively. Graphs have been plotted on load in N vs. displacement in mm for different materials to check their tensile strength and bending strength. For samples PLAT1, PLAT2, and PLAT3 of material PLA, maximum tensile loads are between 4 kN and 4.7 kN and displacements are between 2.3 mm and 2.5 mm, which are shown in the graph in Figure 9. From the graph, it is clear that the PLAT2 sample has the maximum tensile load, which results in the highest ultimate tensile strength among all samples. For samples PLAS1, PLAS2, and PLAS3, maximum bending loads are between 0.35 kN and 0.45 kN, and

displacements are between 4.2 mm and 4.8 mm, which are shown in the graph in Figure 10. From the graph, it is clear that the PLAS1 sample has the highest bending load, which results in maximum bending strength among all samples.

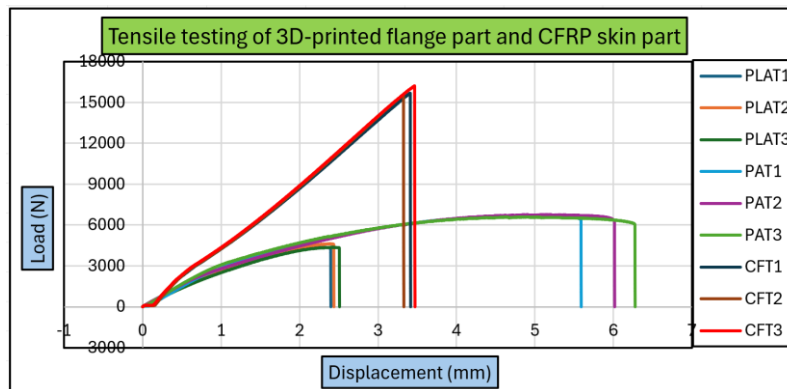


Figure 9: Tensile testing of 3D-printed flange part and CFRP skin part

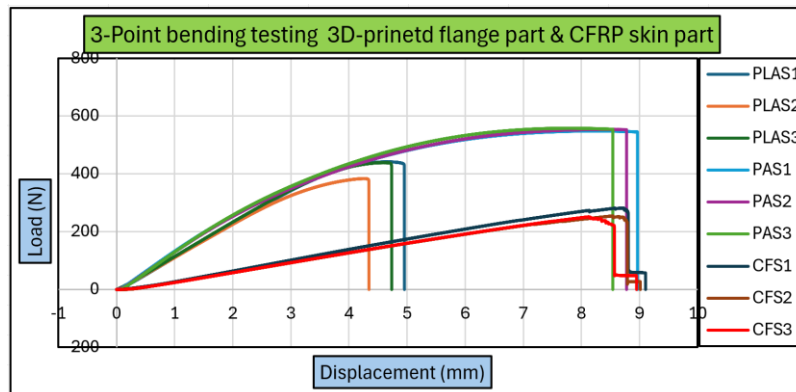


Figure 10: 3-point bending testing of 3D-printed flange part and CFRP skin part

Another material, PA12-CF has been used for testing of tensile strength and bending strength. Three different samples, PAT1, PAT2, and PAT3, have been taken into consideration for comparison of tensile strength. As shown in Figure 9, the maximum tensile load is between 6.5 kN and 6.7 kN, which generates a displacement between 4.8 mm and 5.3 mm. Out of the three samples, the PAT2 sample has the highest tensile load, which is visible in the graph and results in the highest tensile strength among all. Three different samples, PAS1, PAS2, and PAS3, have been taken into consideration for comparison of bending strength. As shown in Figure 10, the maximum bending load is between 0.53 kN and 0.57 kN, which generates a displacement of between 7.5 mm and 8.5 mm. Out of all three samples, the PAS3 sample has the highest bending load, which is visible in the graph and results in the maximum bending strength among all. From the above comparison, it is clear that PA12-CF material has higher tensile strength and bending strength compared to PLA material.

Tensile and bending tests have been performed on CFRP skin parts. Three tensile samples (CFT1, CFT2, and CFT3) were taken into consideration for tensile testing. The maximum

tensile load for these samples is between 15.5 kN and 16.3 kN, which is represented in the graph in Figure 9. From Figure 9, it is clear that CFT3 has the highest tensile load, which results in the highest tensile strength. For bending testing, three samples (CFS1, CFS2, and CFS3) were taken into consideration, as shown in Figure 10. The maximum bending load for samples is between 0.25 kN and 0.29 kN. From Figure 10, CFS1 has the highest bending load, which results in the highest bending strength.

4.2 Simple and modified adhesive-bonded T-joints samples (PLA material):

Tensile Testing:				Shear Testing:			
Samples	Maximum Tensile Load (N)	Displacement (mm)	Ultimate Tensile Strength (MPa)	Samples	Maximum Shear Load (N)	Displacement (mm)	Maximum Shear Strength (MPa)
Simple Adhesive-bonded T-joints Samples (PLA Material):							
PLAST1	1415.92	4.42	39.82	PLASS1	2198.96	11.19	93.23
PLAST2	1650.22	6.31	46.41	PLASS2	2378.25	7.18	100.83
PLAST3	1364.94	3.39	38.38	PLASS3	2665.12	13.93	113.00
Average	1477.02	4.70	41.53	Average	2414.11	10.76	102.35
Modified Adhesive-bonded T-joints Samples (PLA Material):							
PLAMT1	3045.83	4.17	73.99	PLAMS1	5653.22	10.56	197.64
PLAMT2	3615.16	6.20	87.83	PLAMS2	5646.44	8.37	197.41
PLAMT3	3246.82	5.63	78.88	PLAMS3	5294.15	6.79	185.09
Average	3302.60	5.33	80.23	Average	5531.27	8.57	193.38

Table 3: Tensile testing and shear testing of T-joint samples of PLA material

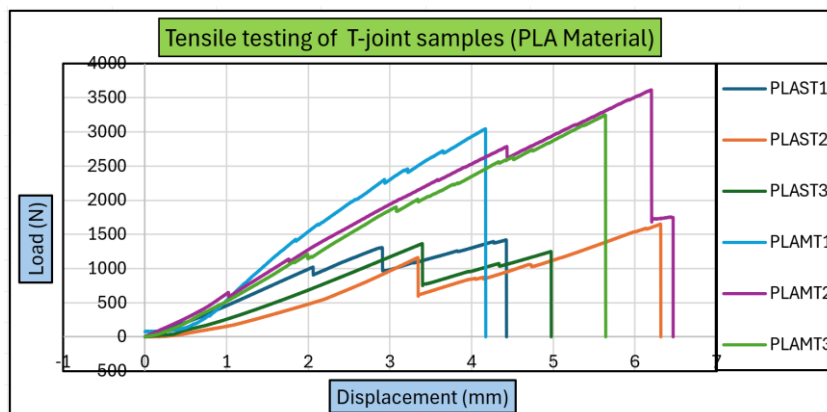


Figure 11: Tensile testing of T-joint samples (PLA material)

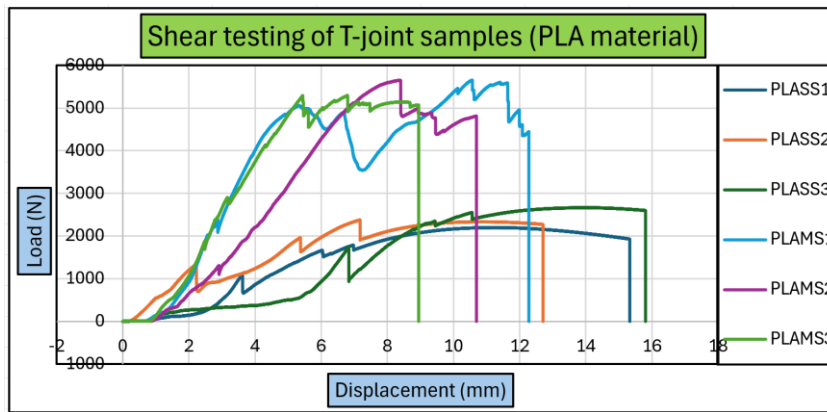


Figure 12: Shear testing of T-joint samples (PLA material)

The performance parameters of simple and modified adhesive-bonded T-joints made of PLA material tested for tensile and shear strength are shown in Table 3. Figure 11 shows tensile testing for samples of simple adhesive-bonded T-joints and modified adhesive-bonded T-joints. From Figure 11, samples PLAST2 of simple adhesive-bonded T-joints and PLAMT2 of modified adhesive-bonded T-joints have the highest tensile load, which results in the highest tensile strengths of 46.41 MPa and 87.83 MPa, respectively.

Figure 12 shows shear testing for samples of simple adhesive-bonded T-joints (PLASS1, PLASS2, PLASS3) and modified adhesive-bonded T-joints (PLAMS1, PLAMS2, PLAMS3). From Figure 12, samples PLASS3 of simple adhesive-bonded T-joints and PLAMS1 of modified adhesive-bonded T-joints have the highest shear load, which results in the highest shear strengths of 113 MPa and 197.64 MPa, respectively.

4.3 Simple and modified adhesive-bonded T-joints samples (PA12-CF material):

Tensile Testing:				Shear Testing:			
Samples	Maximum Tensile Load (N)	Displacement (mm)	Ultimate Tensile Strength (MPa)	Samples	Maximum Shear Load (N)	Displacement (mm)	Maximum Shear Strength (MPa)
Simple Adhesive-bonded T-joints Samples (PA12-CF Material):							
PAST1	971.14	2.95	27.31	PASS1	2417.24	9.30	102.49
PAST2	992.13	2.54	27.90	PASS2	2449.93	8.29	103.87
PAST3	835.26	3.00	23.49	PASS3	2103.78	10.78	89.20
Average	932.84	2.83	26.23	Average	2323.65	9.45	98.52
Modified Adhesive-bonded T-joints Samples (PA12-CF Material):							

PAMT1	2380.43	3.61	57.83	PAMS1	4455.25	5.45	155.76
PAMT2	2589.22	3.54	62.90	PAMS2	4088.32	7.25	142.93
PAMT3	2740.07	3.58	66.57	PAMS3	4318.49	6.98	150.98
Average	2569.90	3.58	62.43	Average	4287.35	6.56	149.89

Table 4: Tensile testing and shear testing T-joint samples of PA12-CF material

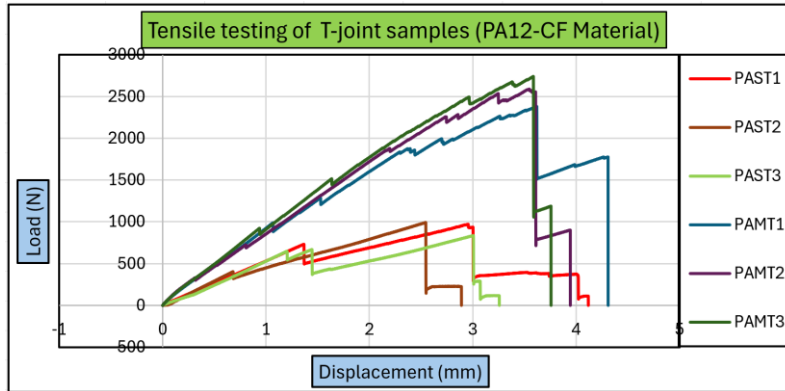


Figure 13: Tensile testing of T-joint samples (PA12-CF material)

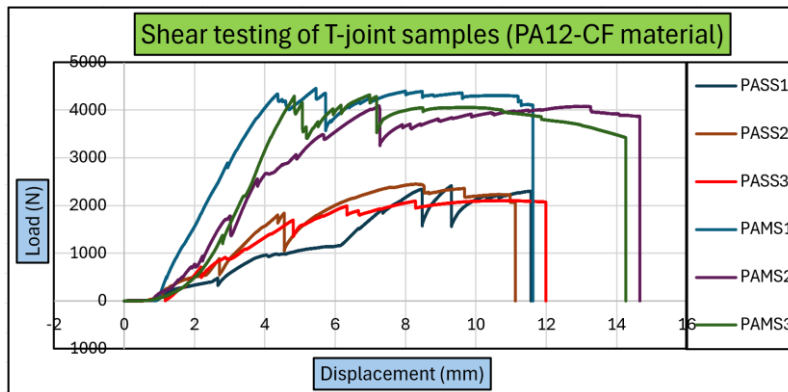


Figure 14: Shear testing of T-joint samples (PA12-CF material)

The tensile testing and shear testing have been performed on PA12-CF material, and their results values are presented in Table 4. Figures 13 and 14 show graphs of the testing results of various samples for tensile testing and shear testing, respectively. For samples PAST1, PAST2, and PAST3, the maximum tensile loads are between 0.83 kN and 1 kN, which are shown in the graph in Figure 13. From the graphs, it is clear that the PAST2 sample has the highest tensile load, which results in the highest ultimate tensile strength among all samples. For samples PASS1, PASS2, and PASS3, the maximum bending loads are between 2.1 kN and 2.5 kN, which are shown in the graph in Figure 14. From the graph, it is clear that the PASS2 sample has the maximum shear load, which results in maximum shear strength among all samples.

Three different samples, PAMT1, PAMT2, and PAMT3, have been taken into consideration for comparison of tensile strength. As shown in Figure 13, the maximum tensile load is

between 2.3 kN and 2.8 kN. Out of all three samples, the PAMT3 sample has the highest tensile load, which is visible in the graph and results in the highest tensile strength among all. Three different samples, PAMS1, PAMS2, and PAMS3, have been taken into consideration for comparison of shear strength. As shown in Figure 14, the maximum shear load is between 4 kN and 4.5 kN. Out of all three samples, the PAMS1 sample has the highest shear load, which is visible in the graph and results in the maximum shear strength among all.

4.4 Electronic Microscopy Images:

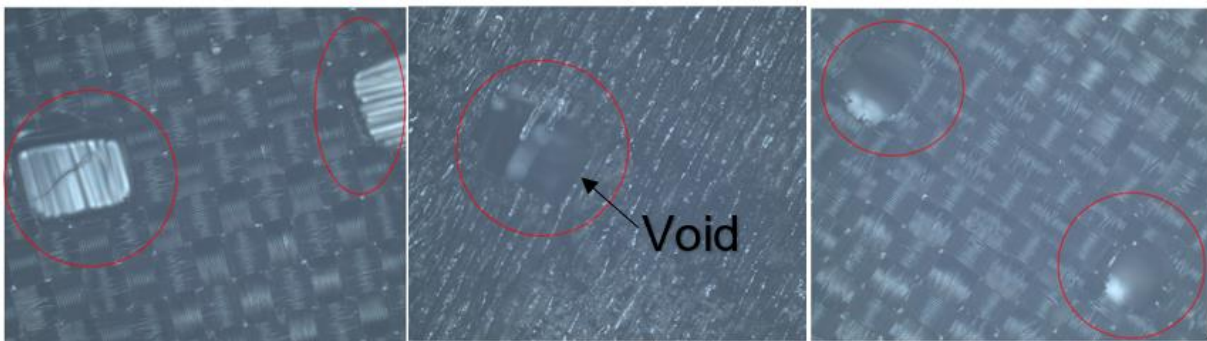


Figure 15: Voids on the adhesive-bonded surface

The electron microscope images give details of the adhesive-bonded surfaces after the tensile and shear testing. During the infused process, the resin flows into the vacuum bags, releasing air bubbles trapped inside the bag. Once the resin solidifies and the adhesive layer cures, it becomes difficult to remove these air bubbles, as illustrated in Figure 15. These voids have a detrimental effect on the bond strength and, as a result, decrease the surface area of contact and the zone of load transfer. These voids are the primary reason for the differences in bonding strength of simple and modified adhesive-bonded T-joints.

5. DISCUSSION

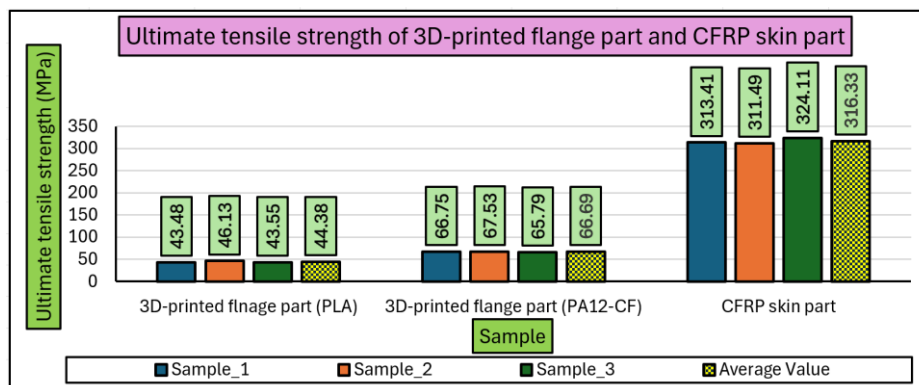


Figure 16: Ultimate tensile strength of 3D-printed flange part and CFRP skin part

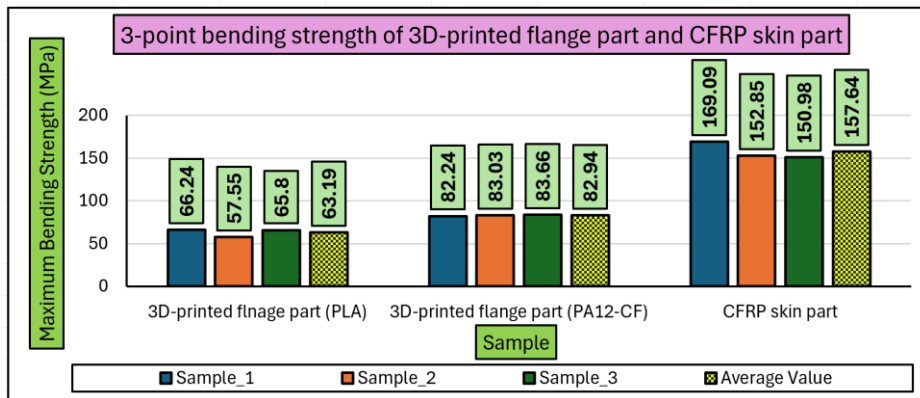


Figure 17: 3-point bending strength of 3D-printed flange part and CFRP skin part

The ultimate tensile strength of the flange part that was printed with PLA and PA12-CF reveals that the two materials performed differently, which is shown in Figure 16. The ultimate tensile strength of the PA12-CF material has a higher average value, which is 66.69 MPa, while the PLA material has an average ultimate tensile strength of 44.38 MPa. This means that, for the same loading rate, PA12-CF material can resist higher tensile forces at failure. In the same way, the 3-point bending test as shown in Figure 17 also pointed out that the PA12-CF material has a higher bending strength (82.94 MPa) than the PLA material (63.19 MPa). PA12-CF material is not only stronger in terms of tension but also offers enhanced flexural capabilities. Moreover, the ultimate tensile strength and bending strength of CFRP skin parts are 316.33 MPa and 157.64 MPa, respectively. The mechanical aspect regarding the tensile and shear strengths of the CFRP skin part proves that the laminated structure utilized for this study exhibits excellent characteristics when subjected to different loading conditions.

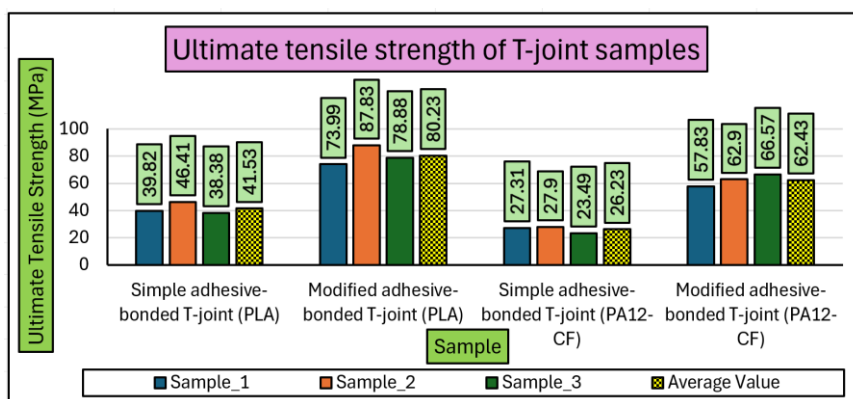


Figure 18: Ultimate tensile strength of T-joint samples

Figure 18 compares the ultimate tensile strength of PLA T-joints with a simple adhesive bond and a modified adhesive bond, demonstrating that the modified adhesive bond does much better than the simple adhesive bond. The average ultimate tensile strength for the simple adhesive-bonded T-joints is 41.53 MPa, whereas for the modified adhesive-bonded

T-joints, it is 80.23 MPa. This represents an increase of approximately 93.18% in ultimate tensile strength for the modified adhesive bond compared to the simple adhesive bond. The modified adhesive-bonded T-joints have a shear strength of 193.38 MPa, which is much higher than the simple adhesive-bonded T-joints' shear strength of 102.35 MPa, as shown in Figure 19. This leads to an approximate 88.93% increase in maximum shear strength for the modified adhesive bond compared to the simple adhesive bond.

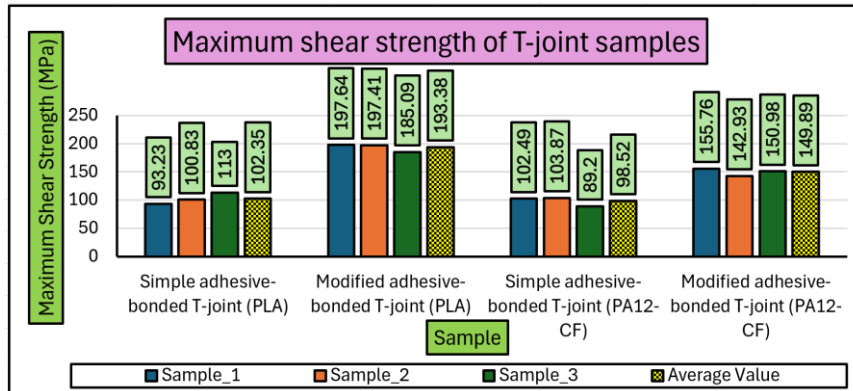


Figure 19: Maximum shear strength of T-joint samples

The ultimate tensile strength of simple and modified adhesive-bonded T-joints made of PA12-CF material was compared in Figure 18. The modified adhesive bond performed much better than the simple adhesive bond, similarly to PLA material. The average ultimate tensile strength for the simple adhesive-bonded T-joints is 26.23 MPa, while for the modified adhesive-bonded T-joints, it is 62.43 MPa. This results in an increase of approximately 137.98% in ultimate tensile strength for the modified adhesive bond compared to the simple adhesive bond. Additionally, when comparing the shear strength shown in Figure 19, the modified adhesive-bonded T-joints exhibit a considerably higher strength with an average of 149.89 MPa, in contrast to the simple adhesive-bonded T-joints (98.52 MPa). This represents an approximate increase of 52.16% in shear strength for the modified adhesive bond over the simple adhesive bond. The comparisons make it clear that the modifications made to the adhesive bond greatly improve both the tensile and shear strengths of the T-joints. This proves that the modified adhesive bond is the better choice for higher mechanical performance applications. Thus, adding one layer of carbon fibre fabric on the flange part creates a stronger bond and enhances the capability of the T-joints to carry loads and provide better structural performance.

The average ultimate tensile strength of PLA material simple adhesive-bonded T-joints (41.53 MPa) and modified adhesive-bonded T-joints (80.23 MPa) is higher compared to the average ultimate tensile strength of PA12-CF material simple adhesive-bonded T-joints (26.23 MPa) and modified adhesive-bonded T-joints (62.43 MPa), as shown in Figure 18.

Similarly, the average shear strength of PLA material simple adhesive-bonded T-joints (102.35 MPa) and modified adhesive-bonded T-joints (193.38 MPa) is also higher compared to the average shear strength of PA12-CF material simple adhesive-bonded T-joints (98.52 MPa) and modified adhesive-bonded T-joints (149.89 MPa), as shown in Figure 19. From the above comparison, PLA material offered better bonding strength in both types of T-joint samples than PA12-CF material. PLA in terms of adhesion, creating a better adhesive bond with carbon fibre fabric and epoxy resin, as shown in Figures 18 and 19. However, the PA12-CF material offered higher tensile and bending strengths than the PLA material, as shown in Figures 16 and 17, but its bonding strength with carbon fibre fabrics was observed to be lower. The adhesive bond surface of the tested PA12-CF T-joint samples revealed stacked short carbon fibre particles on the skin part, potentially contributing to the relatively lower bonding strength of the PA12-CF 3D-printed flange part.

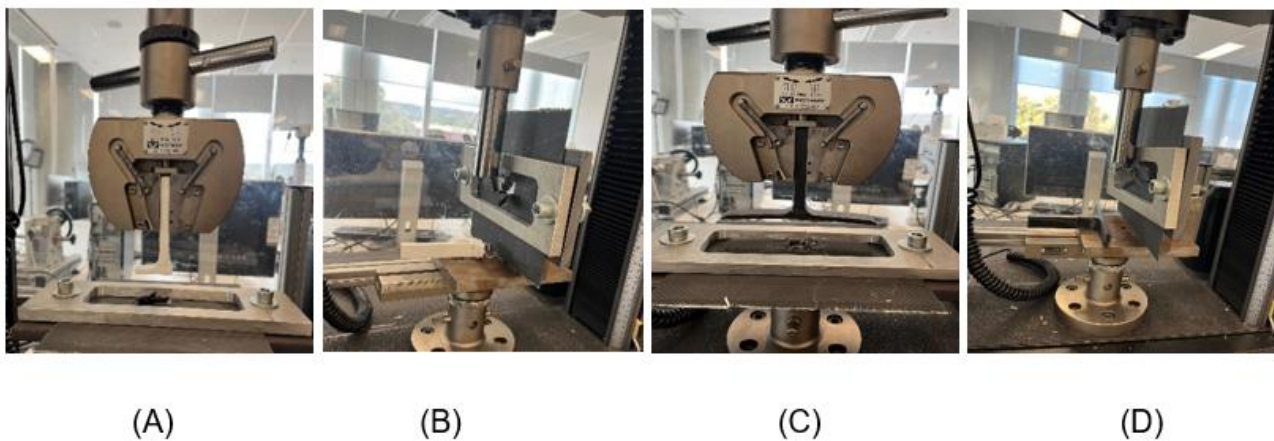


Figure 20: (A) Tensile testing of modified adhesive-bonded T-joints (PLA material) (B) Shear testing of modified adhesive-bonded T-joints (PLA material) (C) Tensile testing of modified adhesive-bonded T-joints (PA12-CF material) (D) Shear testing of modified adhesive-bonded T-joints (PA12-CF material)

During the tensile and shear tests conducted on the adhesive bond samples, significant differences were observed between the simple and modified adhesive-bonded T-joints, fabricated from PLA and PA12-CF materials. At maximum force, tensile and shear forces completely separate the 3D-printed stiffener part from the skin part in simple adhesive-bonded T-joints. However, in the experimental study of modified adhesive bond samples, the PLA material's 3D-printed stiffener part weakened and failed under tensile and shear stresses, as shown in Figures 20 (A) and (B). This is because the stiffener flanges received support from the adhesive bond, together with one carbon fibre fabric layer that is placed on the flanges. On the other hand, during the tensile and shear tests, the PA12-CF material 3D-printed stiffener part completely separated from the skin part without causing any damage to the flanges, which is shown in Figure 20 (C) and (D). When the T-joint samples

experienced a force that bent the PA12-CF material stiffener flanges and broke the modified adhesive bond at the maximum force.

6. FUTURE TRENDS

Advancements in Material Science: In the future, improvements in composite bonding materials may include better mechanical properties, enhanced 3D printing compatibility, and improved performance in various environmental conditions.

The innovative of additive manufacturing: Additive manufacturing advancements can lead to new fabrication patterns, improved composite T-joint structure, and enhanced surface layer precision.

Eco-Friendly Practices: Future trends may then include the idea of creating new environmentally friendly adhesives or fabrication processes that adhere to the principles of sustainability and environmentally friendly materials, as well as incorporating recycling processes into the composite fabrication life cycle.

7. CONCLUSION

This research assessed the adhesive bonding strength characteristics of composite T-joint structures with stiffener sections fabricated using 3D printing and the skin section being CFRP laminates. The adhesive bonding is achieved through the VARTM process. The tensile and bending strengths of PA-12 CF and PLA material-based stiffener sections were assessed through mechanical testing. It was observed that PA-12 CF had significantly greater tensile strength and bending compared to PLA. However, PLA exhibited greater adhesive bonding strength with CFRP laminates.

The test results from tensile and shear tests of simple and modified adhesive bonds indicate that the bonding strength is considerably greater in modified adhesive bonds. These results indicate that incorporating a single layer of carbon fibre fabric over the flange section improves the bond strength and makes the T-joints more suitable for real-world applications.

REFERENCES

- [1] Hamitouche, L., Tarfaoui, M., & Vautrin, A. (2009). Design and test of a sandwich T-joint for naval ships. *Damage and Fracture Mechanics: Failure Analysis of Engineering Materials and Structures*, 131-141. https://link.springer.com/chapter/10.1007/978-90-481-2669-9_14
- [2] Stickler, P.B. and Ramulu, M., 2001. Investigation of mechanical behavior of transverse stitched T-joints with PR520 resin in flexure and tension. *Composite structures*, 52(3-4), pp.307-314. <https://www.sciencedirect.com/science/article/abs/pii/S026382230100023X>
- [3] Sandanamsamy, L., Mogan, J., Rajan, K., Harun, W.S.W., Ishak, I., Romlay, F.R.M., Samykano, M. and Kadirgama, K., 2023. Effect of process parameter on tensile properties of FDM printed PLA. *Materials Today: Proceedings*. <https://www.sciencedirect.com/science/article/pii/S2214785323012592>
- [4] Pejkowski, Ł., Seyda, J., Nowicki, K. and Mroziak, D., 2023. Mechanical performance of non-reinforced, carbon fiber reinforced, and glass bubbles reinforced 3D printed PA12 polyamide. *Polymer Testing*, 118, p.107891. <https://www.sciencedirect.com/science/article/pii/S0142941822004123>
- [5] Patel, H., & Dave, H. (2023). The effect of stacking sequence and fiber orientation on tensile and flexural strength of fiber reinforced composite fabricated by VARTM process. *Engineering Solid Mechanics*, 11(1), 47-62. <http://m.growingscience.com/beta/esm/5715-the-effect-of-stacking-sequence-and-fiber-orientation-on-tensile-and-flexural-strength-of-fiber-reinforced-composite-fabricated-by-vartm-process.html>
- [6] Tamakuwala, V.R., 2021. Manufacturing of fiber reinforced polymer by using VARTM process: A review. *Materials Today: Proceedings*, 44, pp.987-993. <https://www.sciencedirect.com/science/article/pii/S2214785320387083>
- [7] Dahmen, V., Redmann, A.J., Austermann, J., Quintanilla, A.L., Mecham, S.J. and Osswald, T.A., 2020. Fabrication of hybrid composite T-joints by co-curing with 3D printed dual cure epoxy. *Composites Part B: Engineering*, 183, p.107728. <https://www.sciencedirect.com/science/article/abs/pii/S1359836819335693>

- [8] Liu, Y., Li, M., Lu, X. and Zhu, X., 2021. Failure mechanism and strength prediction model of T-joint of composite sandwich structure. *Metals*, 11(8), p.1197.
<https://www.researchgate.net/publication/353498179> Failure Mechanism and Strength Prediction Model of T-Joint of Composite Sandwich Structure
- [9] Cardoso, J., Nunes-Pereira, J. and Silva, A., 2018. Fabrication of adhesively bonded CFRP T-joints for stiffener pull-off tests. <https://ubibliorum.ubi.pt/handle/10400.6/14086>
- [10] Sápi, Zsombor. (2019). Design, analysis, and testing of composite T-joints.
<https://www.researchgate.net/publication/335603080> Design analysis and testing of composite T-joints
- [11] Cope, R.D. & Pipes, Byron. (1982). Design of the composite spar-wingskin joint. *Composites*. 13. 47-53. 10.1016/0010-4361(82)90170-7.
<https://www.researchgate.net/publication/248364613> Design of the composite spar-wingskin joint
- [12] Zhang, J., Zhao, L., Qin, T., Fu, Y. and Fei, B., 2014. Influence of π overlaminates on the mechanical behavior of all-composite adhesively bonded π joints. *Journal of Reinforced Plastics and Composites*, 33(10), pp.923-934.
<https://journals.sagepub.com/doi/abs/10.1177/0731684414522331?journalCode=jrpa>
- [13] Hiremath, V.S., Dhilipkumar, T., Reddy, D.M. and Bagewadi, S., 2023. Effect of print orientation on tensile and shear properties of 3D printed lap joints. *Materials Today: Proceedings*. <https://www.sciencedirect.com/science/article/pii/S2214785323037550>
- [14] Kumar, A. and Kumar, D., 2022. Vacuum assisted resin transfer Moulding process review and variability analysis using Taguchi optimization technique. *Materials Today: Proceedings*, 50, pp.1472-1479.
<https://www.sciencedirect.com/science/article/pii/S221478532105851X>
- [15] Sun, Z., Chen, H., Song, Z., Liu, H., Cui, R., Guo, X. and Shi, S., 2021. Three-point bending properties of carbon fiber/honeycomb sandwich panels with short-fiber tissue and carbon-fiber belt interfacial toughening at different loading rate. *Composites Part A: Applied Science and Manufacturing*, 143, p.106289.
<https://www.sciencedirect.com/science/article/pii/S1359835X21000191>

- [16] Zhao, J. and Zhu, J., 2011. Electron microscopy and in situ testing of mechanical deformation of carbon nanotubes. *Micron*, 42(7), pp.663-679.
<https://www.sciencedirect.com/science/article/pii/S0968432811000631>
- [17] Carbon fibre reinforcement sheet material.
<https://atlcomposites.com.au/product/159/Carbon-Reinforcements>
- [18] Resin Part A: KINETIX RD246 , Hardner Part B: Material: KINETIX HD160
<https://atlcomposites.com.au/icart/products/22/images/main/KINETIX%20R246%20LV.pdf>
- [19] PolyLite™ PLA/ 1.75mm/ Regular/ White/ 1k
<https://www.3dprintingsolutions.com.au/Store/Australia/polylite-pla-3d-filament/polylite-pla-white-1kg>
- [20] PolyMide™ PA12-CF/2.85mm/Black/500g
<https://www.3dprintingsolutions.com.au/Store/Australia/nylon-12-cf-filament/polymide-pa12-cf-black-500g/285mm>
- [21] Ravindran, A.R., Ladani, R.B., Wang, C.H. and Mouritz, A.P., 2022. Hierarchical strengthening of carbon fibre composite T-joints using nanoparticles and Z-pins. *Composites Part A: Applied Science and Manufacturing*, 154, p.106775.
<https://www.sciencedirect.com/science/article/pii/S1359835X21004851>
- [22] Md. Sakib Hasan, 2023. Determination of Tensile Strength of a given specimen using UTM (25KN).
https://www.researchgate.net/publication/373679769_Determination_of_Tensile_Strength_of_a_given_specimen_using_UTM_25KN
- [23] Wikipedia Contributors. (2019, May 11). *Flexural strength*. Wikipedia; Wikimedia Foundation. https://en.wikipedia.org/wiki/Flexural_strength
- [24] Wang, Y., Soutis, C., Hajdaei, A. and Hogg, P.J., 2015. Finite element analysis of composite T-joints used in wind turbine blades. *Plastics, Rubber and Composites*, 44(3), pp.87-97.
https://www.researchgate.net/publication/325533819_Finite_element_analysis_of_composite_T-joints_used_in_wind_turbine_blades_effect_of_interlaminar_veils_and_stitching
- [25] *Weld Stress Calculations - Roy Mech*. (n.d.). Roymech.org.
https://roymech.org/Useful_Tables/Form/Weld_strength.html

APPENDICES

1. Research Timeline Gantt Chart:

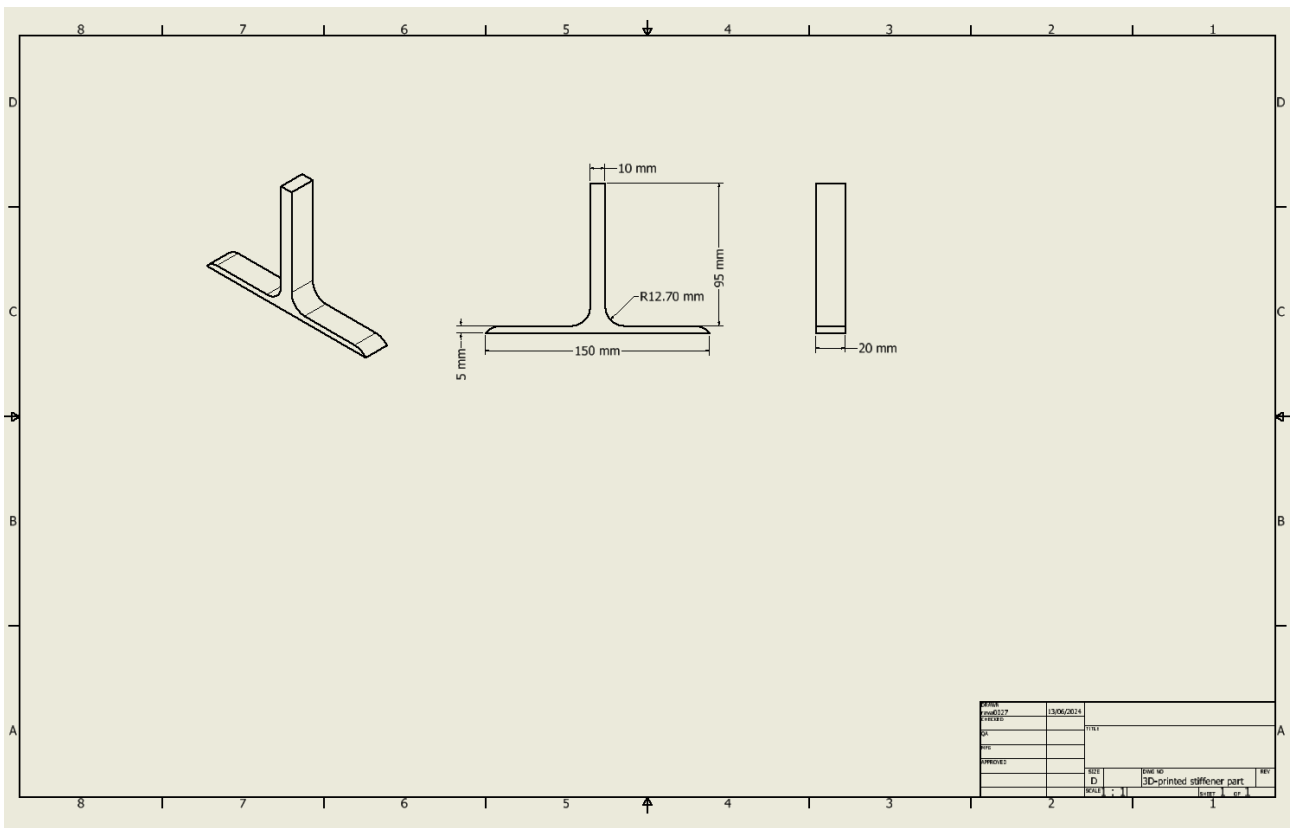
Semester 1, Start: 26 Feb 2024 End: 13 Jun 2024																		
Task No.	Task Description	Week 1	Week 2	Week 3	Week 4	Week 5	Week 6	Break	Week 7	Week 8	Week 9	Week 10	Week 11	Week 12	Week 13	Week 14	Week 15	Week 16
1	Project meetings	█																
2	Literature Review		█	█	█	█	█											
3	3D Modelling				█													
4	Training for 3D printing					█												
5	Manufacturing 3D printed stiffener and flang parts					█	█	█	█									
6	Thesis summary submission								█									
7	VARTM process training									█								
8	Manufacturing T-joint samples									█	█	█	█	█				
9	Sample testing										█	█	█	█				
10	Data Collection										█	█	█	█				
11	Results Seminar											█						
12	Data Analysis											█	█	█				
13	Methodology and Research Plan Submission													█				
14	Final Report														█	█	█	█

2. Risk assessment form

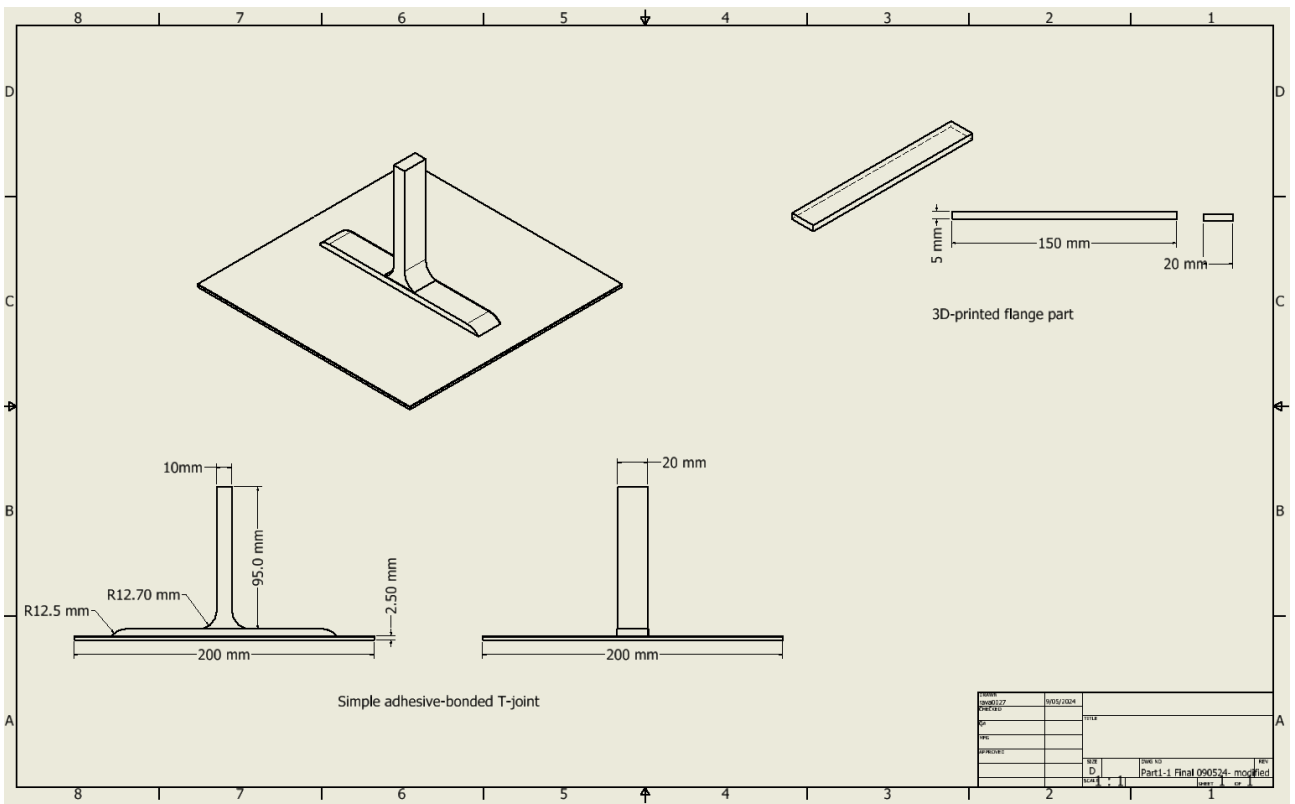
College/Portfolio	Flinders University	Area/Unit	G.07,3.19	Location	Tonsley campus	Area/Unit Manager	Tim Hodge
Task/Procedure	VARTM manufacture and mechanical testing of test specimens.	Workers consulted / involved	Tim Hodge	Date	26/03/2024	Review Date	28/03/2024

Identified Hazard before controls		Risk Assessment			Risk Controls	Residual risk			Implementation
No.	Description	Consequences	Likelihood	Risk Measure (see matrix)	Control measures	Consequences	Likelihood	Risk Measure (see matrix)	Date controls implemented / reviewed
1	Exposure to chemicals	Minor Injury	Possible	Medium	Use Personal Protective equipment such as safety goggles, coats, and gloves while conducting experiments and manufacturing.	First Aid	Unlikely	Medium	26/03/2024
2	Slips, Trips and falls	Minor Injury	Likely	Medium	Always wear closed-toe shoes in the laboratory. Clean spills immediately.	First Aid	Possible	Medium	27/03/2024
3	Measurement data loss from corrupted drive.	Negligible	Likely	Medium	Data derived from the Instron testing machine and experiments are immediately backed up in physical format and in OneDrive to avoid data loss.	Negligible	Highly Unlikely	Low	26/03/2024
4	Fabricated test specimen damage due to improper mounting on the universal testing machine.	Negligible	Likely	Medium	Specially designed platforms for the Universal testing machine are designed and fabricated to secure the test specimens during testing and avoid any damage.	Negligible	Unlikely	Low	26/03/2024
5	Imperfections like voids and dry-spots in test specimens manufactured using Vacuum-assisted resin transfer molding procedure leading to false data results.	Negligible	Likely	Medium	Procedure parameters are investigated from existing literature and manufacture is carried out as per specified conditions to avoid dry-spots and voids.	Negligible	Unlikely	Low	28/03/2024

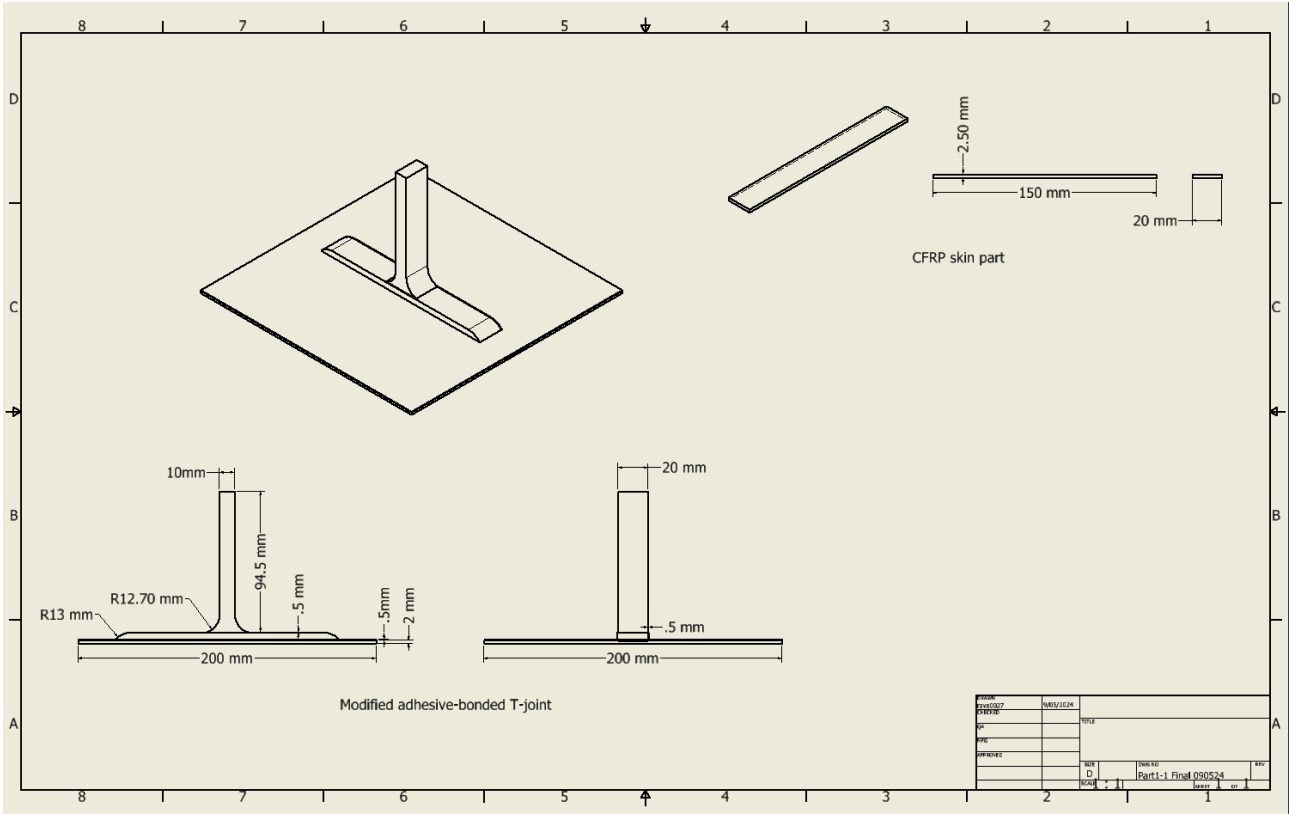
3. Engineering drawing of 3D-printed stiffener part



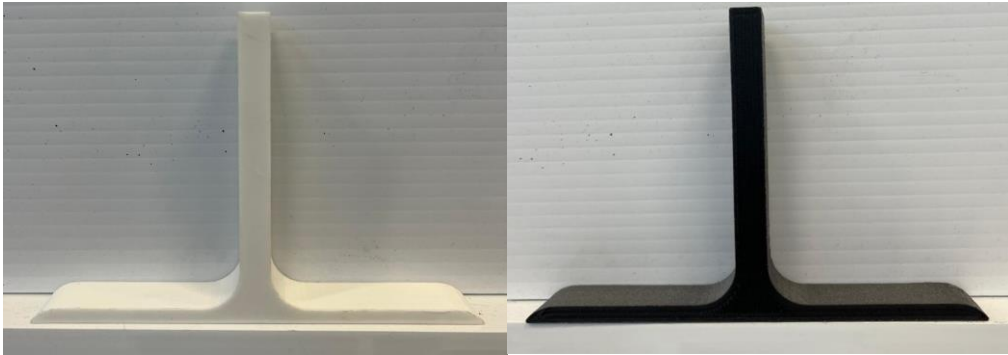
4. Engineering drawing of simple adhesive-bonded T-joint and 3D-printed flange part



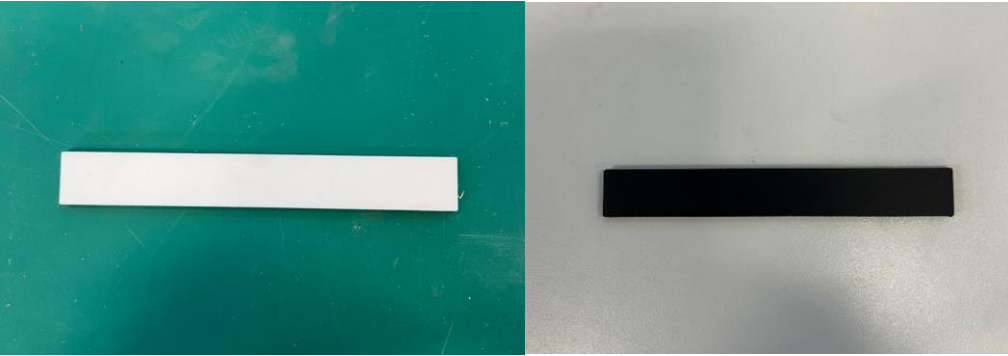
5. Engineering drawing of modified adhesive-bonded T-joint and CFRP skin part



6. 3D printed stiffener part of the PLA in white and PA12-CF in black.



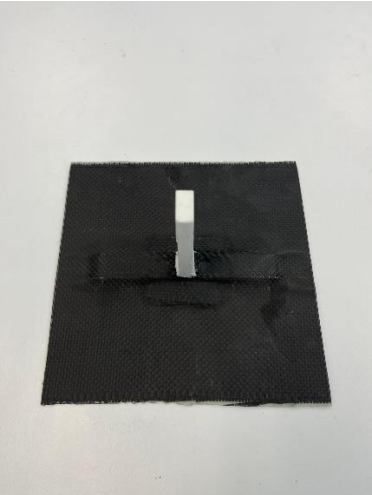
7. 3D printed flange part of the PLA in white and PA12-CF in black.



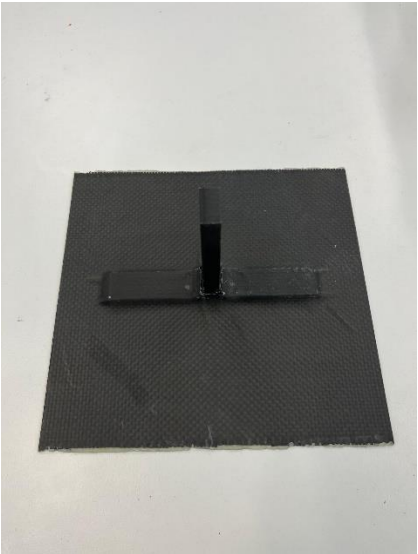
8. Simple adhesive-bonded T-joint of PLA material



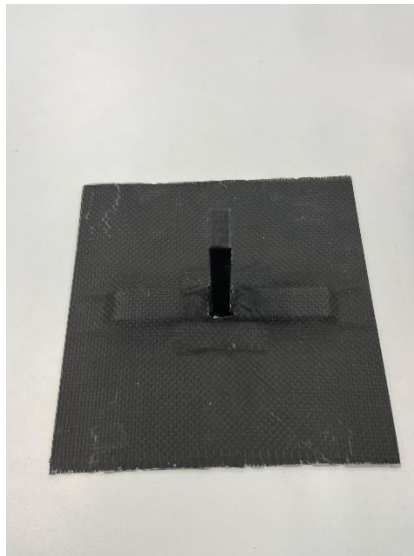
9. Modified adhesive-bonded T-joint of PLA material



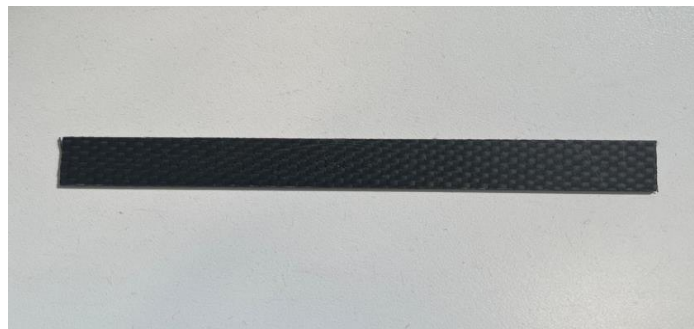
10. Simple adhesive-bonded T-joint of PA12-CF material







11. Modified adhesive-bonded T-joint of PA12-CF material

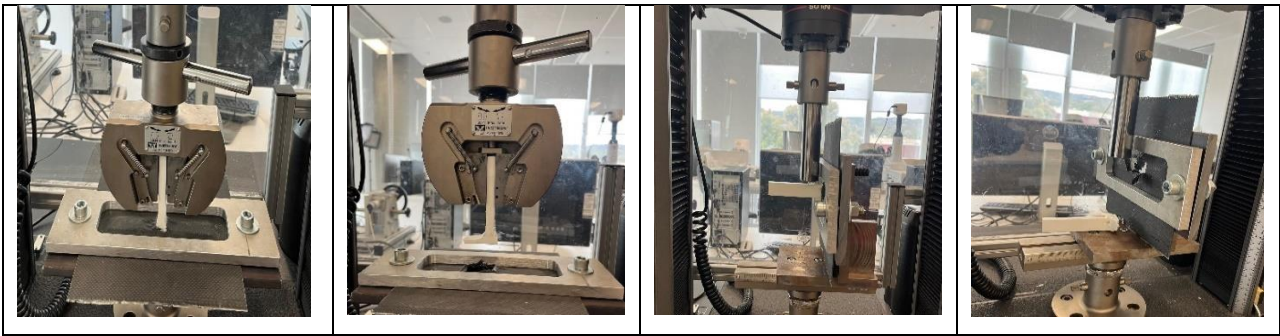


12. CFRP skin part







13. PLA material T-joint samples behaviour in tensile and shear testing.

Simple adhesive-bonded T-joint samples (PLA Material):			
Tensile Testing:		Shear Testing:	
Before Testing	After Testing	Before Testing	After Testing
			
Modified adhesive-bonded T-joint samples (PLA Material):			
Tensile Testing:		Shear Testing:	
Before Testing	After Testing	Before Testing	After Testing



1. PA12-CF material T-joint samples behaviour in tensile and shear testing.

Simple adhesive-bonded T-joint samples (PA12-CF Material)			
Tensile Testing		Shear testing	
Before Testing	After Testing	Before Testing	After Testing
			
Modified adhesive-bonded T-joint samples (PA12-CF Material)			
Tensile Testing		Shear Testing	
Before Testing	After Testing	Before Testing	After Testing
